photonics

IMPACT FACTOR 2.536

CITESCORE 2.3

Communication

Method for the Quantum Metric Tensor Measurement in a Continuous Variable System

Ling-Shan Lin, Hao-Long Zhang and Zhen-Biao Yang

Special Issue

Nonlinear and Quantum Optics in Coupled Structures: Fundamentals and Applications

Edited by

Dr. Bing He and Dr. Jianming Wen

MDPI

https://doi.org/10.3390/photonics10030256

photonics

MDPI

Communication

Method for the Quantum Metric Tensor Measurement in a Continuous Variable System

Ling-Shan Lin, Hao-Long Zhang and Zhen-Biao Yang *

Fujian Key Laboratory of Quantum Information and Quantum Optics, College of Physics and Information Engineering, Fuzhou University, Fuzhou 350116, China
* Correspondence: zbyang@fzu.edu.cn

Abstract: As a fundamental concept, geometry is widely used in understanding physical phenomena. In quantum mechanics, geometry is related to the system's quantum state and can be characterized by the quantum geometric tensor (QGT), whose real part is referred to as the quantum metric tensor (QMT), which defines the distance between two neighboring quantum states in the projected Hilbert space. Several pieces of research based on discrete variables have been proposed to extract the QMT, but research with the use of continuous variables is lacking. Here, we propose a method to extract the QMT of a continuous variable system, specified here as a cat-qubit. The method is developed by constructing the Kerr nonlinear parametric oscillator (KNPO) and by modulating it with external drives to induce adiabatic dynamics process within the state subspace spanned by the even and odd *Schödinger* cat states. The method paves the way for exploring the geometry for continuous variable systems.

Keywords: quantum metric tensor; continuous variable systems; cat-qubit

Citation: Lin, L.-S.; Zhang, H.-L.; Yang, Z.-B. Method for the Quantum Metric Tensor Measurement in a Continuous Variable System. *Photonics* **2023**, *10*, 256. https://doi.org/10.3390/photonics10030256

Received: 5 January 2023
Revised: 16 February 2023
Accepted: 27 February 2023
Published: 28 February 2023

1. Introduction

Geometry is a critical concept for describing fundamental principles of nature. In the quantum world, quantum states are presented by the wavefunctions in Hilbert space with specific dimensions, quantum geometry builds the geometric construction in this space [1–3].

The quantum geometric tensor (QGT) [4–8] provides a powerful tool to outline the geometry of Hilbert space. On one hand, its imaginary part, Berry curvature, is widely explored for understanding various physical phenomena, such as the Aharonov–Bohm effect [9], the Berry phase [10–14] and the topology of condensed matter [15–20]. On the other hand, the real part defines the quantum metric tensor (QMT), which reflects the quantum distance between two neighboring quantum states in the parametric space. What is more, as a gauge invariable, the QMT has been widely exploited in various studies, such as quantum fluctuations [21–24], quantum phase transition [25–29] and topological matter [30]. It is also associated with a topological invariant, the Euler characteristic number [2,6,31–33], for describing the topology of the state manifold. So, it is pivotal to measure the QMT for analyzing the geometry of the quantum system.

So far, theoretical and experimental studies have been conducted to measure the QMT in different physical systems [33–41]. However, schemes to measure this intriguing quantity in a continuous variable system are still lacking. Here, we propose a scheme to measure the QMT in a continuous variable system with cat-qubit encoding [42–46]. We consider a superconducting quantum interference device (SQUID) array [47] to construct the Kerr nonlinear parametric oscillator (KNPO) [48–52] for stabilizing the Schrödinger cat states, together by inducing two modulated drives and controlling the detuning of the oscillator to realize an effective and modulated two-level system, with a pair of continuous variable even and odd schrödinger cat states as the encoding bases. Through the method of adiabatic

control of the KNPO system's state evolution in the parametric space, we numerically analyze and extract the QMT. The results are highly consistent with the theory, providing an effective method with which to explore the geometry of continuous variable systems.

2. Quantum Metric Tensorl (QMT)

We consider a Hamiltonian $\hat{H}(\mathbf{r})$ of a nondegenerate quantum system, which is dependent on N dimensionless parameters $\mathbf{r} = (r_1, r_2, \ldots, r_N)^{Tr}$, and define the corresponding eigensystem:

$$\hat{H}(\mathbf{r})|u_k(\mathbf{r})\rangle = E_k(\mathbf{r})|u_k(\mathbf{r})\rangle, \tag{1}$$

where $|u_k(\mathbf{r})\rangle$ and $E_k(\mathbf{r})$ are the eigenstate and the eigenenergy with quantum number k, respectively. By projecting these dynamics onto this nondegenerate band $E_k(\mathbf{r})$, we can define the QGT of this geometric construction as (see Appendix A):

$$Q_{ij}^k = \langle \partial_i u_k(\mathbf{r})|(1 - |u_k(\mathbf{r})\rangle\langle u_k(\mathbf{r})|)|\partial_j u_k(\mathbf{r})\rangle, \tag{2}$$

with $i, j \in \{r_1, r_2, \ldots, r_N\}$. Note that the QGT is complex, and can be spanned into two parts. The imaginary part is related to the Berry curvature: $\mathrm{Im}\{Q_{ij}\} = -F_{ij}/2$, which is anti-symmetric; while the real part defines quantum metric tensor: $\mathrm{Re}\{Q_{ij}\} = g_{ij}$, which is symmetric.

For two nearby quantum states $|\psi(\mathbf{r})\rangle$ and $|\psi(\mathbf{r} + \mathbf{dr})\rangle$, the QMT defines the distance of them in the corresponding parametric space:

$$ds^2 = 1 - |\langle\psi(\mathbf{r})|\psi(\mathbf{r} + \mathbf{dr})\rangle|^2 = \sum_{ij} g_{ij} dr_i dr_j. \tag{3}$$

As shown in Figure 1, this quantity gives the geometric picture in the parametric space, where it expresses the length of the geodesic curve between two neighboring quantum states in the parametric space, reflecting the fluctuation of the system for the corresponding Hamiltonian. What is more, it can be exploited to present the excited probability of the eigenstate for the parameter-dependent Hamiltonian $\hat{H}(\mathbf{r})$, which is the core of our method to extract the QMT of the continuous variable quantum system.

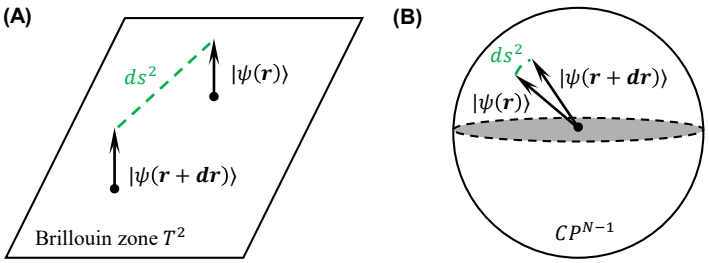

Figure 1. Illustration of the distance between two nearby quantum states in the parametric space. (**A**) The geometric picture of quantum distance in Brillouin zone T^2. (**B**) The geometric picture of quantum distance on Bloch sphere.

3. The KNPO as the Continuous Variable System

We realize the continuous variable system by considering the model in ref. [47]. This model consists of a large capacitor and N Josephson junctions, with the use of the high-frequency magnetic flux to construct the SQUID array.

As shown in Figure 2, the corresponding Hamiltonian is ($\hbar = 1$ is set):

$$\hat{H}_{SQUID} = 4E_C\hat{n}^2 - NE_J(\Phi(t))\cos\frac{\hat{\phi}}{N}, \tag{4}$$

where $\hat{n}$ is the number of Cooper pairs and $\hat{\phi}$ is the phase over the Josephson junctions array, E_C is the charging energy including shunt capacitor and parasitic capacitance of Josephson junctions and E_J is the Josephson energy for the SQUID array controlled by the external flux $\Phi(t)$. This flux is harmonically modulated around its mean value with a small amplitude, so $E_J(\Phi(t))$ can be approximated as $E_J + \delta E_J \cos \omega_m t$, where ω_m is the harmonic frequency. Since $\hat{\phi}$ is a small quantity (see Appendix B), we can make the Taylor expansion to the second term and drop the high-order terms. Due to the commutation relation $[\hat{\phi}, \hat{n}] = i\hbar$, we can rewrite this Hamiltonian using bosonic operators $\hat{a}$ and $\hat{a}^\dagger$:

$$\hat{H}_{bosonic} = \omega_c \hat{a}^\dagger \hat{a} + \frac{K}{6}(\hat{a} + \hat{a}^\dagger)^4 - [2P(\hat{a} + \hat{a}^\dagger)^2 + \frac{4KP}{3\omega_c}(\hat{a} + \hat{a}^\dagger)^4] \cos \omega_m t, \tag{5}$$

where $\hat{n}$ and $\hat{\phi}$ are expressed by the bosonic operators $\hat{a}$ and $\hat{a}^\dagger$: $\hat{n} = (\frac{E_J}{32NE_C})^{\frac{1}{4}} i(\hat{a}^\dagger - \hat{a})$ and $\hat{\phi} = (\frac{2NE_C}{E_J})^{\frac{1}{4}}(\hat{a}^\dagger + \hat{a})$, $\omega_c = \sqrt{8E_C E_J/N}$, $K = -E_C/2N^2$ and $P = -\omega_c \delta E_J/8E_J$. Here, K and P correspond to the Kerr-nonlinearity and the pump strength of the KNPO, respectively. We control $4KP \ll 3\omega_c$ to drop the last term, turn into the rotating frame at the frequency $\omega_m/2$, and drop the high-frequency terms according to the rotating wave approximation. The effective Hamiltonian is:

$$\hat{H}_{eff} = K\hat{a}^{\dagger 2}\hat{a}^2 + \Delta \hat{a}^\dagger \hat{a} - P(\hat{a}^2 + \hat{a}^{\dagger 2}), \tag{6}$$

with $\Delta = \omega_c + 2K - \omega_m/2$. The constructed KPNO system dominated by the Hamiltonian (6) possesses two degenerate ground states of the continuous variable kind, i.e., the even and odd Schrödinger cat states:

$$\begin{aligned} |C^+\rangle &= N_+(|+\alpha\rangle + |-\alpha\rangle), \\ |C^-\rangle &= N_-(|+\alpha\rangle - |-\alpha\rangle), \end{aligned} \tag{7}$$

where $\alpha = \sqrt{P/K}$ and $N_\pm = \frac{1}{(2 \pm 2e^{-2|\alpha|^2})^{1/2}}$.

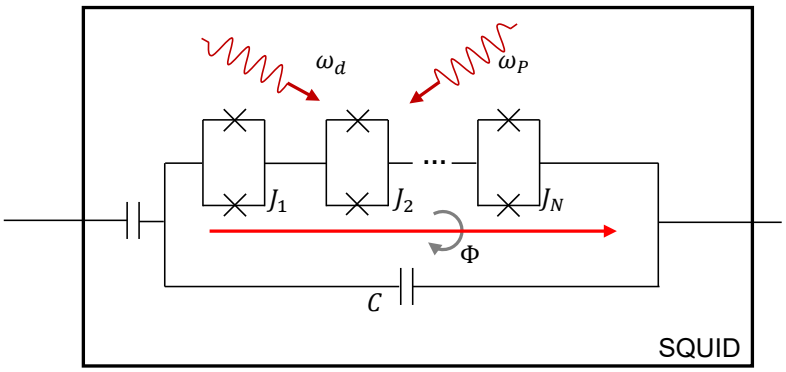

Figure 2. Circuit diagram of the KNPO. The red and gray arrows denote the external flux and the magnetic field, respectively, while two red wave arrows represent the modulated drives.

4. Arbitrary Manipulation of the Continuous Variable System

We now turn to the discussion of the arbitrary manipulation of the continuous variable system, with the full Hamiltonian modelled as:

$$\begin{aligned} \hat{H}_{full} = &\quad K\hat{a}^{\dagger 2}\hat{a}^2 - P(\hat{a}^2 + \hat{a}^{\dagger 2}) + \Delta \hat{a}^\dagger \hat{a} + \hat{H}_d, \\ \hat{H}_d = &\quad 2\epsilon_x \cos \omega_d t(\hat{a}^\dagger + \hat{a}) + 2\epsilon_y \cos \omega_p t(\hat{a}^\dagger - \hat{a}), \end{aligned} \tag{8}$$

where $\epsilon_{x/y}$ and $\omega_{d/p}$ are the amplitudes and the angular frequencies of the drives, respectively. We let $\omega_d = \omega_p = \omega_{shift}$ and rotate into the frame of $\hat{H}_0 = \frac{\omega_{shift}}{2}\hat{a}^\dagger \hat{a} + K\hat{a}^{\dagger 2}\hat{a}^2 -$

$P(\hat{a}^2 + \hat{a}^{\dagger 2})$. By neglecting the high-order oscillation terms, we then rewrite the Hamiltonian in the basis of cat states:

$$\hat{H}_{two} = \Omega_x \hat{\tilde{\sigma}}_x + \Omega_y \hat{\tilde{\sigma}}_y + \Omega_z \hat{\tilde{\sigma}}_z, \tag{9}$$

with

$$\begin{aligned} \Omega_x &= 4\alpha N_- N_+ \epsilon_x, \\ \Omega_y &= -4\epsilon_y \alpha N_- N_+ e^{-2|\alpha|^2} i, \\ \Omega_z &= (\Delta - \omega_{shift}) 8|\alpha|^2 N_+^2 N_-^2 e^{-2|\alpha|^2}, \end{aligned} \tag{10}$$

where $\hat{\tilde{\sigma}}_i$ $(i \in \{x, y, z\})$ are the Pauli operators defined with the continuous variable state space $\{|C^+\rangle, |C^-\rangle\}$. It should be noted that $e^{-2|\alpha|^2}$ is an exponential function about average photon number $|\alpha|^2$ of the cat state component, so the amplitude of coherent state $|\alpha|$ should be small. What is more, to evade the high-level leakage, we should keep Ω_y and Ω_z small. According to the formula of the effective two-level system, we let $\Omega_z = \frac{\Omega}{2}\cos\theta$, $\Omega_x = \frac{\Omega}{2}\sin\theta\cos\phi$, and $\Omega_y = \frac{\Omega}{2}\sin\theta\sin\phi$, with $\theta \in [0, \pi], \phi \in [0, 2\pi]$.

To check the stability of this system, we performed the simple numerical simulation, by initialing the system's state in the ground eigenstate of $\hat{H}_{two}(\theta = \frac{\pi}{4}, \phi = 0)$ and adiabatically evolving this system into $\hat{H}_{two}(\theta = \frac{\pi}{4} + d\theta, \phi = 0)$, where $d\theta = \pi/32$. Note that the numerical calculations are performed through the truncation of the infinite-dimension Fock basis state Hilbert space to the dimension of 20. For the duration with the large enough $T \gg 1/(P^2/K)$, the system with the initial state will adiabatically evolve along $|u^+(\mathbf{r})\rangle$ to reach a final state. In Figure 3B, we show the fidelity $|\langle u^+(\mathbf{r})|\psi(t)\rangle|^2$ as a function of the variable θ for the set of reasonably chosen parameters, with the numerical results well consistent with the theory for a large enough T. For the cases with the reduced evolution time T, the fidelity is slightly deviated, as also depicted in Figure 3B.

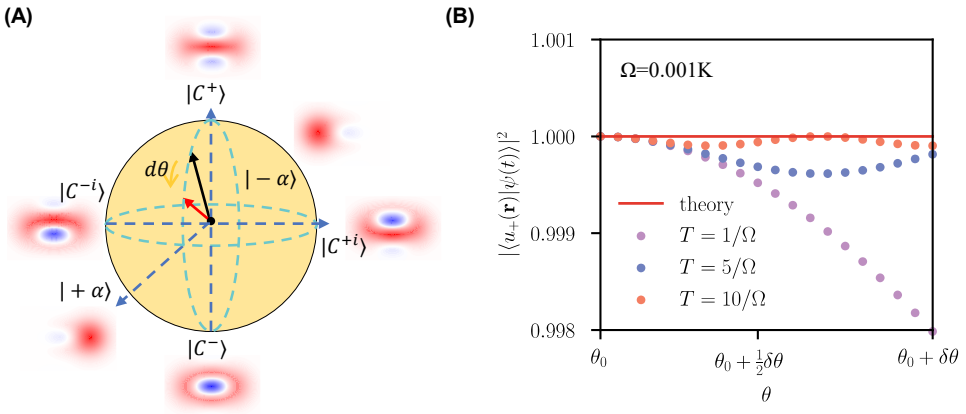

Figure 3. The dynamics process of the adiabatic evolution. (**A**) The Bloch dynamics process of the adiabatic evolution. The Wigner functions of the states at the six cardinal points on the sphere (defined with the cat-qubit) are shown. $|C^\pm\rangle = N_\pm(|+\alpha\rangle \pm |-\alpha\rangle)$, where $N_\pm$ is normalization factor. Similarly, $|C^{\pm i}\rangle = N_{\pm i}(|+\alpha\rangle \mp i|-\alpha\rangle)$. (**B**) The fidelities for the numerical and theoretical results, respectively, with $\theta_0 = \pi/4$, $\phi_0 = 0$ and $\delta\theta = \pi/32$, $\Omega = 0.001K$, $P = K$, $T = 100/\Omega$, $\mathbf{r} = (\sin\theta\cos\phi, \sin\theta\sin\phi, \cos\theta)$, $|u^+(\mathbf{r})\rangle = \cos\frac{\theta}{2}|C^+\rangle + \sin\frac{\theta}{2}e^{i\phi}|C^-\rangle$ and $|\psi(t)\rangle$ is the quantum state in the evolution.

5. Method for the Measurement of the QMT

To extract the QMT, we use the definition of quantum distance (see Appendix C of ref. [39]). First, we make a single-parametric modulation to the Hamiltonian $\hat{H}(\mathbf{r} + \frac{t}{T}\delta r_i \mathbf{e}_i)$ and set the initial state the eigenstate state of the initial Hamiltonian $\hat{H}(\mathbf{r})$ with quantum number k. After the adiabatic evolution with the period T, we measure the

excited probability $P_{ii}^k = 1 - \left|\langle u_k(\mathbf{r} + \frac{t}{T}\delta r_i \mathbf{e}_i)|\psi(t)\rangle\right|^2$, which can be achieved by mapping the continuous variable basis state to the Fock qubit and followed by dispersive readout [50]. According to the Equation (3), we can obtain the diagonal elements of the QMT:

$$g_{ii}^k = \frac{P_{ii}^k}{dr_i^2}. \tag{11}$$

We then make two-parametric modulation $\hat{H}(\mathbf{r} + \frac{t}{T}\delta r_i \mathbf{e}_i + \frac{t}{T}\delta r_j \mathbf{e}_j)$ and $\hat{H}(\mathbf{r} + \frac{t}{T}\delta r_i \mathbf{e}_i - \frac{t}{T}\delta r_j \mathbf{e}_j)$ to measure the corresponding probability $P_{ij}^{k+} = g_{ii}^k dr_i^2 + 2g_{ij}^k dr_i dr_j + g_{jj}^k dr_j^2$ and $P_{ij}^{k-} = g_{ii}^k dr_i^2 - 2g_{ij}^k dr_i dr_j + g_{jj}^k dr_j^2$. These two probabilities can be exploited to calculate the off-diagonal elements of the QMT:

$$g_{ij}^k = \frac{P_{ij}^{k+} - P_{ij}^{k-}}{4dr_i dr_j}. \tag{12}$$

Numerical simulations are performed to verify this theory. Note that, for the numerical calculations, the infinite-dimension Fock basis state Hilbert space is truncated to the dimension of 20, for the set of reasonably chosen parameters. We consider the effective two-level Hamiltonian:

$$\hat{H}(\theta, \phi) = \frac{\Omega}{2}\begin{pmatrix} \cos\theta & \sin\theta e^{-i\phi} \\ \sin\theta e^{i\phi} & -\cos\theta \end{pmatrix}, \tag{13}$$

which can be constructed in Equation (9), with the effective ground state $|u_-\rangle = \sin\frac{\theta}{2}|C^+\rangle - \cos\frac{\theta}{2}e^{i\phi}|C^-\rangle$ and the effective excited state $|u_+\rangle = \cos\frac{\theta}{2}|C^+\rangle + \sin\frac{\theta}{2}e^{i\phi}|C^-\rangle$. By substituting them into Equation (2), we get the QMT:

$$g_\pm = \mathrm{Re}\{Q\} = \begin{pmatrix} \frac{1}{4} & 0 \\ 0 & \frac{1}{4}\sin^2\theta \end{pmatrix}. \tag{14}$$

Here, we initialize the quantum state in the ground state of the Hamiltonian $\hat{H}(\theta_0, \phi_0)$, perform two single-parametric modulations $\hat{H}(\theta_0 + \frac{t}{T}\delta\theta, \phi_0)$ and $\hat{H}(\theta_0, \phi_0 + \frac{t}{T}\delta\phi)$ to calculate the diagonal elements of the QMT, and two two-parametric modulations $\hat{H}(\theta_0 + \frac{t}{T}\delta\theta, \phi_0 + \frac{t}{T}\delta\phi)$ and $\hat{H}(\theta_0 + \frac{t}{T}\delta\theta, \phi_0 - \frac{t}{T}\delta\phi)$ to calculate the off-diagonal elements of the QMT.

The numerical results are shown in Figure 4, which displays the elements of the QMT as the function of the initial condition θ_0 (here we set $\phi_0 = 0$), showing the accordance between the theoretical (solid lines) and numerical (dots) results.

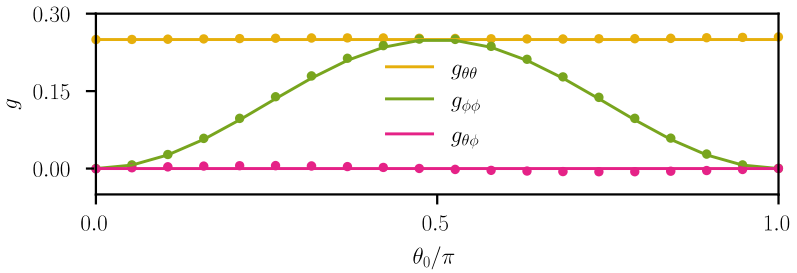

Figure 4. Extraction of the QMT of the continuous variable system. The numerical results of the QMT $g_{\theta\theta}$ (yellow dots), $g_{\phi\phi}$ (green dots), and $g_{\theta\phi}$ (pink dots) are plotted with the theoretical results (solid lines). The whole adiabatic evolution is simulated with $\Omega = 0.001K$, $P = K$, $\delta\theta = \delta\phi = \frac{\pi}{32}$ and $T = 100/\Omega$.

6. Discussion and Conclusions

In summary, we have proposed a new scheme for the measurement of the QMT with a modulated KNPO system, achieved first by the adiabatic manipulation of the KNPO within the parametric space defined with the continuous variable Schrödinger even and odd cat state bases, and followed by the acquirement of the excited probabilities. The numerical calculations were performed by the adoption of the continuous variable system states defined in the truncated indefinite-dimensional Fock state Hilbert space, and by use of the reasonably chosen parameters.

The measurement of the QMT based on the modulated KNPO system can be, in principle, achieved by use of a microwave-driving superconducting nonlinear inductive element [50]. As compared with the previously demonstrated methods that adopt the discrete two-level solid-state systems [39–41], our method provides an alternative for the exploration of geometry and its relevant topology with quantum physical systems, and can be extended to reveal the geometry and topology with interacting [40,41] or high-dimensional [53,54] continuous variable systems.

Author Contributions: Z.-B.Y. conceived the idea. L.-S.L. and H.-L.Z. derived the analytical solution and performed the numerical simulation under the supervision of Z.-B.Y., H.-L.Z. and Z.-B.Y. cowrote the manuscript. All authors have read and agreed to the published version of the manuscript.

Funding: This research was funded by the National Natural Science Foundation of China (Grant No. 11875108).

Institutional Review Board Statement: Not applicable.

Informed Consent Statement: Not applicable.

Data Availability Statement: All data generated or analysed for this study are available on reasonable request.

Conflicts of Interest: The authors declare no conflict of interest.

Abbreviations

The following abbreviations are used in this manuscript:

QGT	quantum geometric tensor
KNPO	Kerr nonlinear parametric oscillator
SQUID	superconducting quantum interference device
ECN	Euler characteristic number

Appendix A. Quantum Geometric Tensor

For some quantum states in the infinite dimensional Hilbert space, we can take it into the projected Hilbert space due to the gauge invariability ($|\psi\rangle = e^{i\alpha}|\psi\rangle$), and then build the relative geometric structure. Studies along this path are often named geometric quantum mechanics.

Geometric quantum mechanics have two critical structures, which are described by quantum geometric tensor (QGT). The first one is the metric structure, corresponding to the real part of the QGT, i.e., QMT (or Fubini-study metric), that defines the quantum distance between two different states; the other one is the gauge structure, which is the imaginary part of the QGT related to the gauge field, i.e, Berry curvature.

To define the QGT, we consider a family of parameter-dependent Hamiltonian $\hat{H}_{\vec{r}}$ requiring a smooth dependence on a set of parameters $\vec{r} = (r_1, r_2, \ldots)^{Tr}$. The parameters $\vec{r}$ construct the projected Hilbert space $\mathcal{H}(\vec{r})$. If the eigenenergy and the eigenstate are denoted by $E_n(\vec{r})$ and $|u_n\rangle(\vec{r})$, respectively, the quantum states of this system can be represented as:

$$|\psi(\vec{r})\rangle = \sum_i a_i |u_i(\vec{r})\rangle. \tag{A1}$$

Upon infinitesimal variation of the parameter $d\vec{r}$, we can define the quantum distance:

$$ds^2 = ||\psi(\vec{r}+d\vec{r}) - \psi(\vec{r})||^2 = \langle\delta\psi|\delta\psi\rangle = \sum_{ij}\langle\partial_i\psi|\partial_j\psi\rangle dr_i dr_j, \tag{A2}$$

and define $\langle\partial_i\psi|\partial_j\psi\rangle = \gamma_{ij} + i\sigma_{ij}$. It can be proved that $(\langle\partial_i\psi|\partial_j\psi\rangle)^* = \gamma_{ij} - i\sigma_{ij} = \langle\partial_j\psi|\partial_i\psi\rangle = \gamma_{ji} + i\sigma_{ji}$, so $\sum_{ij}\sigma_{ij} = 0$. We then rewrite the quantum distance:

$$ds^2 = \sum_{ij}\gamma_{ij}dr_i dr_j. \tag{A3}$$

However, we can't define γ_{ij} as the metric structure because it is not gauge invariant. For example, we let $|\psi\rangle' = e^{i\alpha(\vec{r})}|\psi\rangle$, with $|\psi\rangle'$ and $|\psi\rangle$ referring to as the same quantum state, then we see the corresponding γ'_{ij}:

$$\gamma'_{ij} = \langle\partial_i\psi|\partial_j\psi\rangle - \beta_i\partial_j\alpha - \beta_j\partial_i\alpha + \partial_i\alpha\partial_j\alpha, \tag{A4}$$

where $\beta_i = i\langle\psi|\partial_i\psi\rangle$ is the Berry connection, which is purely real ($\beta_i^* = -i\langle\partial_i\psi|\psi\rangle = i\langle\psi|\partial_i\psi\rangle = \beta_i$). It can be seen that $\gamma_{ij} \neq \gamma'_{ij}$. The rescue is to redefine a gauge invariant metric $g_{ij} = \gamma_{ij} - \beta_i\beta_j$ to let $g_{ij} = g'_{ij}$. In this case, g does not measure the distance of states in Hilbert space $\mathcal{H}$, but measure the distance of 'Rays' in projected Hilbert space $\mathcal{PH} = \mathcal{H}/U(1)$. It is reasonable because the physical observable relates to Hermitean operators acting on 'Rays', required by the principle of gauge invariance. So we define the QGT as:

$$\chi_{ij} = \gamma_{ij} + i\sigma_{ij} - \beta_i\beta_j = \langle\partial_i\psi|(1 - |\psi\rangle\langle\psi|)|\partial_j\psi\rangle. \tag{A5}$$

The corresponding metric and gauge structures are:

$$g_{ij} = \mathrm{Re}\{\chi_{ij}\};\ \sigma_{ij} = \mathrm{Im}\{\chi_{ij}\}. \tag{A6}$$

Then to define the quantum distance in projected Hilbert space $|\tilde{\psi}\rangle = e^{i\alpha(\vec{r})}|\psi\rangle$, where α is arbitrarily complex, we select the minimal distance in this subspace:

$$D^2(\tilde{\psi_1}, \tilde{\psi_2}) = \min_{\alpha_1,\alpha_2}\left|\left|\psi_1 e^{i\alpha_1} - \psi_2 e^{i\alpha_2}\right|\right| = 2 - 2|\langle\psi_1|\psi_2\rangle|. \tag{A7}$$

We further consider two nearby quantum states $|\psi(\vec{r})\rangle$ and $|\psi(\vec{r}+d\vec{r})\rangle$, upon infinitesimal variation $d\vec{r}$, and do Taylor expansion of $|\psi(\vec{r}+d\vec{r})\rangle$:

$$\begin{aligned} |\psi(\vec{r}+d\vec{r})\rangle &= |\psi(\vec{r})\rangle + \textstyle\sum_i|\partial_i\psi(\vec{r})\rangle dr_i + \frac{1}{2}\sum_{ij}\langle\psi|\partial_i\partial_j\psi\rangle dr_i dr_j + \mathcal{O}(dr^3) \\ &= |\psi(\vec{r})\rangle + \textstyle\sum_i|\partial_i\psi(\vec{r})\rangle dr_i - \frac{1}{2}\sum_{ij}\langle\partial_i\psi|\partial_j\psi\rangle dr_i dr_j + \mathcal{O}(dr^3), \end{aligned} \tag{A8}$$

and calculate $|\langle\psi(\vec{r})|\psi(\vec{r}+d\vec{r})\rangle|^2$:

$$\begin{aligned} |\langle\psi(\vec{r})|\psi(\vec{r}+d\vec{r})\rangle|^2 = \quad & 1 + \textstyle\sum_i\langle\psi|\partial_i\psi\rangle dr_i - \frac{1}{2}\sum_{ij}\langle\partial_i\psi|\partial_j\psi\rangle dr_i dr_j + \sum_i\langle\partial_i\psi|\psi\rangle dr_i + \\ & \textstyle\sum_{ij}\langle\partial_i|\psi\rangle\langle\psi|\partial_j\psi\rangle dr_i dr_j - \frac{1}{2}\sum_{ij}\langle\partial_i\psi|\partial_j\psi\rangle + \mathcal{O}(dr^3). \end{aligned} \tag{A9}$$

Neglecting the high-order infinitesimal, we can obtain:

$$|\langle\psi(\vec{r})|\psi(\vec{r}+d\vec{r})\rangle|^2 \approx \left|1 - \frac{1}{2}\sum_{ij}g_{ij}dr_i dr_j\right|^2, \tag{A10}$$

and calculate the distance:

$$ds^2 = 2 - 2|\langle\psi(\vec{r})|\psi(\vec{r}+d\vec{r})\rangle| = \sum_{ij} g_{ij} dr_i dr_j, \tag{A11}$$

which is called geodesic quantum distance, meaning the effective distance between two nearby quantum states in the projected Hilbert space. It is worth noticing that the inner product of any two states should be within the range of $[0, 1]$, by which we regard the QGT as a metric measuring the geodesic distance of points lying on the Bloch sphere. Specifically, if we define $|\langle\psi(\vec{r})|\psi(\vec{r}+d\vec{r})\rangle| = \cos\frac{\theta}{2}$, then $d\theta = 2ds = 2\sqrt{|g_{ij}dr_i dr_j|}$.

What's more, we can write the geodesic quantum distance in the other formula:

$$ds^2 = \sum_{ij} g_{ij} dr_i dr_j = 1 - |\langle\psi(\vec{r})|\psi(\vec{r}+d\vec{r})\rangle|^2. \tag{A12}$$

Appendix B. Kerr Nonlinear Parametric Oscillator

To engineer the KNPO, we consider a SQUID-array resonator with N SQUIDs (As shown in Figure 2), whose effective Hamiltonian can be written as ($\hbar = 1$):

$$\hat{H} = 4E_c\hat{n}^2 - NE_J[\Phi(t)]\cos\frac{\hat{\phi}}{N}, \tag{A13}$$

where $\hat{n}$ and $\hat{\phi}$ are the number of Cooper pairs and overall phase across the junction array, respectively, E_c is the resonator's charging energy including the contribution of the junction capacitance C_J^i, $i = 1, 2, 3, \ldots, N$, and the shunt capacitance C, N is the number of SQUIDs in the array, and E_J is Josephson energy for a single SQUID in the array, depending on the external flux $\Phi(t)$, which can be expressed as $E_J + \delta E_J \cos\omega_m t$.

Similar to the transmon, we can expend $\cos\frac{\hat{\phi}}{N}$ in the Equation (A13):

$$\hat{H} = 4E_c\hat{n}^2 - NE_J[1 - \frac{1}{2}(\frac{\hat{\phi}}{N})^2 + \frac{1}{24}(\frac{\hat{\phi}}{N})^4 + \mathcal{O}(\hat{\phi}^6)] - N\delta E_J[1 - \frac{1}{2}(\frac{\hat{\phi}}{N})^2 + \frac{1}{24}(\frac{\hat{\phi}}{N})^4 + \mathcal{O}(\hat{\phi}^6)]. \tag{A14}$$

We then induce the annihilation and creation operators to substitute $\hat{n}$ and $\hat{\phi}$:

$$\begin{aligned} \hat{n} &= n_0 \cdot i(\hat{a}^\dagger - \hat{a}), \\ \hat{\phi} &= \phi_0 \cdot (\hat{a}^\dagger + \hat{a}). \end{aligned} \tag{A15}$$

with $n_0 = (E_J/32NE_c)^{\frac{1}{4}}$ and $\phi_0 = (2NE_c/E_J)^{\frac{1}{4}}$ being the zero-point fluctuations. After the quantization and by ignoring the constant terms, we obtain the Hamiltonian of the SQUID array resonator:

$$\hat{H} = \omega_c\hat{a}^\dagger\hat{a} + \frac{K}{6}(\hat{a} + \hat{a}^\dagger)^4 - [2P(\hat{a} + \hat{a}^\dagger)^2 + \frac{4KP}{3\omega_c^{(0)}}(\hat{a} + \hat{a}^\dagger)^4]\cos\omega_m t, \tag{A16}$$

where $\omega_c = \sqrt{8E_cE_J/N}$, $K = -E_c/2N^2$ and $P = -\omega_c^{(0)}\delta E_J/8E_J$. Here K and P correspond to the Kerr-nonlinearity coefficient and pump strength, respectively. Let $4KP \ll 3\omega_c^{(0)}$, we can neglect the last term. Therefore, the effective Hamiltonian can be written as:

$$\hat{H} = \omega_c\hat{a}^\dagger\hat{a} + \frac{K}{6}(\hat{a} + \hat{a}^\dagger)^4 - P(\hat{a} + \hat{a}^\dagger)^2(e^{i\omega_m t} + e^{-i\omega_m t}). \tag{A17}$$

By moving into a rotating frame at the frequency of $\omega_m/2$ and neglecting the high-frequency terms according to the RWA, the final Hamiltonian is reduced to:

$$\hat{H} = K\hat{a}^{\dagger 2}\hat{a}^2 + \Delta\hat{a}^\dagger\hat{a} - P(\hat{a}^2 + \hat{a}^2). \tag{A18}$$

where $\Delta = \omega_c + 2K - \omega_m/2$. This Hamiltonian describes a Kerr non-linear oscillator with the two-photon driving and the Kerr nonlinearity. To make the Taylor expansion, it's required $\hat{\phi}$ to be infinitesimal to satisfy this condition:

$$\phi_{class} = \min\{\langle\hat{\phi}\rangle + \sqrt{\langle\hat{\phi}^2\rangle - \langle\hat{\phi}\rangle^2}\} = \phi_0 = \sqrt{2NE_c/E_J}. \tag{A19}$$

We can choose the large capacitance C to make E_c a little quantity (equivalent to the transmon model), and thus to drop the last term in Equation (A16):

$$4KP \ll 3\omega_c \rightarrow \delta E_J \ll \frac{12E_JE_c}{N^2}. \tag{A20}$$

This means that the applied external magnetic flux is weak. Finally, to drop the high-frequency terms in the Equation (A17), we should make the frequency of the external magnetic large. It is like a transmon model with a weak but high-frequency cosine-oscillation magnetic field. The two-photon squeezing drive is applied by this magnetic field, while the Kerr nonlinearity originates from the anharmonicity of the transmon model.

References

1. Kibble, T.W.B. Geometrization of quantum mechanics. *Commun. Math. Phys.* **1979**, *65*, 189–201. [CrossRef]
2. Anandan, J.; Aharonov, Y. Geometry of quantum evolution. *Phys. Rev. Lett.* **1990**, *65*, 1697–1700. [CrossRef] [PubMed]
3. Brody, D.C.; Hughston, L.P. Geometric quantum mechanics. *J. Geom. Phys.* **2001**, *38*, 19–53. [CrossRef]
4. Kolodrubetz, M.; Sels, D.; Mehta, P.; Polkovnikov, A. Geometry and non-adiabatic response in quantum and classical systems. *Phys. Rep.* **2017**, *697*, 1–87. [CrossRef]
5. Campos Venuti, L.; Zanardi, P. Quantum Critical Scaling of the Geometric Tensors. *Phys. Rev. Lett.* **2007**, *99*, 095701. [CrossRef]
6. Ma, Y.Q.; Chen, S.; Fan, H.; Liu, W.M. Abelian and non-Abelian quantum geometric tensor. *Phys. Rev. B* **2010**, *81*, 245129. [CrossRef]
7. Cheng, R. Quantum Geometric Tensor (Fubini-Study Metric) in Simple Quantum system. *arXiv* **2013**, arXiv:1502.03551.
8. Provost, J.P.; Vallee, G. Riemannian structure on manifolds of quantum states. *Commun. Math. Phys.* **1980**, *76*, 289–301. [CrossRef]
9. Aharonov, Y.; Bohm, D. Significance of Electromagnetic Potentials in the Quantum Theory. *Phys. Rev.* **1959**, *115*, 485–491. [CrossRef]
10. Xiao, D.; Chang, M.C.; Niu, Q. Berry phase effects on electronic properties. *Rev. Mod. Phys.* **2010**, *82*, 1959–2007. [CrossRef]
11. Bohm, A.R.; Mostafazadeh, A.; Koizumi, H.; Niu, Q.; Zwanziger, J. *The Geometric Phase in Quantum Systems: Foundations, Mathematical Concepts, and Applications in Molecular and Condensed Matter Physics*; Springer: Berlin/Heidelberg, Germany, 2003.
12. Pachos, J.; Zanardi, P.; Rasetti, M. Non-Abelian Berry connections for quantum computation. *Phys. Rev. A* **1999**, *61*, 010305. [CrossRef]
13. Zanardi, P.; Rasetti, M. Holonomic quantum computation. *Phys. Lett. A* **1999**, *264*, 94–99. [CrossRef]
14. Berry, M.V. Quantal phase factors accompanying adiabatic changes. *Proc. R. Soc. Lond. A Math. Phys. Sci.* **1984**, *392*, 45–57. [CrossRef]
15. Hasan, M.Z.; Kane, C.L. Colloquium: Topological insulators. *Rev. Mod. Phys.* **2010**, *82*, 3045–3067. [CrossRef]
16. Wen, X.G. Mean-field theory of spin-liquid states with finite energy gap and topological orders. *Phys. Rev. B* **1991**, *44*, 2664–2672. [CrossRef]
17. Wen, X.G. Colloquium: Zoo of quantum-topological phases of matter. *Rev. Mod. Phys.* **2017**, *89*, 041004. [CrossRef]
18. Zhang, D.W.; Zhu, Y.Q.; Zhao, Y.X.; Yan, H.; Zhu, S.L. Topological quantum matter with cold atoms. *Adv. Phys.* **2018**, *67*, 253–402. [CrossRef]
19. Qi, X.L.; Zhang, S.C. Topological insulators and superconductors. *Rev. Mod. Phys.* **2011**, *83*, 1057–1110. [CrossRef]
20. Armitage, N.; Mele, E.; Vishwanath, A. Weyl and Dirac semimetals in three-dimensional solids. *Rev. Mod. Phys.* **2018**, *90*, 015001. [CrossRef]
21. Wootters, W.K. Statistical distance and Hilbert space. *Phys. Rev. D* **1981**, *23*, 357–362. [CrossRef]
22. Braunstein, S.L.; Caves, C.M. Statistical distance and the geometry of quantum states. *Phys. Rev. Lett.* **1994**, *72*, 3439–3443. [CrossRef]
23. Souza, I.; Wilkens, T.; Martin, R.M. Polarization and localization in insulators: Generating function approach. *Phys. Rev. B* **2000**, *62*, 1666–1683. [CrossRef]
24. Ozawa, T.; Goldman, N. Probing localization and quantum geometry by spectroscopy. *Phys. Rev. Res.* **2019**, *1*, 032019. [CrossRef]
25. Roy, R. Band geometry of fractional topological insulators. *Phys. Rev. B* **2014**, *90*, 165139. [CrossRef]
26. Lim, L.K.; Fuchs, J.N.; Montambaux, G. Geometry of Bloch states probed by Stückelberg interferometry. *Phys. Rev. A* **2015**, *92*, 063627. [CrossRef]

27. Palumbo, G.; Goldman, N. Revealing Tensor Monopoles through Quantum-Metric Measurements. *Phys. Rev. Lett.* **2018**, *121*, 170401. [CrossRef]
28. Zanardi, P.; Paunković, N. Ground state overlap and quantum phase transitions. *Phys. Rev. E* **2006**, *74*, 031123. [CrossRef]
29. Carollo, A.; Valenti, D.; Spagnolo, B. Geometry of quantum phase transitions. *Phys. Rep.* **2020**, *838*, 1–72. [CrossRef]
30. Zanardi, P.; Giorda, P.; Cozzini, M. Information-Theoretic Differential Geometry of Quantum Phase Transitions. *Phys. Rev. Lett.* **2007**, *99*, 100603. [CrossRef]
31. Rezakhani, A.T.; Abasto, D.F.; Lidar, D.A.; Zanardi, P. Intrinsic geometry of quantum adiabatic evolution and quantum phase transitions. *Phys. Rev. A* **2010**, *82*, 012321. [CrossRef]
32. Ma, Y.Q.; Gu, S.J.; Chen, S.; Fan, H.; Liu, W.M. The Euler number of Bloch states manifold and the quantum phases in gapped fermionic systems. *Europhys. Lett.* **2013**, *103*, 10008. [CrossRef]
33. Kolodrubetz, M.; Gritsev, V.; Polkovnikov, A. Classifying and measuring geometry of a quantum ground state manifold. *Phys. Rev. B* **2013**, *88*, 064304. [CrossRef]
34. Neupert, T.; Chamon, C.; Mudry, C. Measuring the quantum geometry of Bloch bands with current noise. *Phys. Rev. B* **2013**, *87*, 245103. [CrossRef]
35. Ozawa, T. Steady-state Hall response and quantum geometry of driven-dissipative lattices. *Phys. Rev. B* **2018**, *97*, 041108. [CrossRef]
36. Bleu, O.; Malpuech, G.; Gao, Y.; Solnyshkov, D. Effective Theory of Nonadiabatic Quantum Evolution Based on the Quantum Geometric Tensor. *Phys. Rev. Lett.* **2018**, *121*, 020401. [CrossRef] [PubMed]
37. Bleu, O.; Solnyshkov, D.D.; Malpuech, G. Measuring the quantum geometric tensor in two-dimensional photonic and exciton-polariton systems. *Phys. Rev. B* **2018**, *97*, 195422. [CrossRef]
38. Klees, R.; Rastelli, G.; Cuevas, J.; Belzig, W. Microwave Spectroscopy Reveals the Quantum Geometric Tensor of Topological Josephson Matter. *Phys. Rev. Lett.* **2020**, *124*, 197002. [CrossRef]
39. Tan, X.; Zhang, D.W.; Yang, Z.; Chu, J.; Zhu, Y.Q.; Li, D.; Yang, X.; Song, S.; Han, Z.; Li, Z.; et al. Experimental Measurement of the Quantum Metric Tensor and Related Topological Phase Transition with a Superconducting Qubit. *Phys. Rev. Lett.* **2019**, *122*, 210401. . [CrossRef] [PubMed]
40. Zheng, W.; Xu, J.; Ma, Z.; Li, Y.; Dong, Y.; Zhang, Y.; Wang, X.; Sun, G.; Wu, P.; Zhao, J.; et al. Measuring Quantum Geometric Tensor of Non-Abelian System in Superconducting Circuits. *Chin. Phys. Lett.* **2022**, *39*, 100202. [CrossRef]
41. Yu, M.; Yang, P.; Gong, M.; Cao, Q.; Lu, Q.; Liu, H.; Zhang, S.; Plenio, M.B.; Jelezko, F.; Ozawa, T.; et al. Experimental measurement of the quantum geometric tensor using coupled qubits in diamond. *Natl. Sci. Rev.* **2019**, *7*, 254–260. [CrossRef] [PubMed]
42. Chamberland, C.; Noh, K.; Arrangoiz-Arriola, P.; Campbell, E.T.; Hann, C.T.; Iverson, J.; Putterman, H.; Bohdanowicz, T.C.; Flammia, S.T.; Keller, A.; et al. Building a Fault-Tolerant Quantum Computer Using Concatenated Cat Codes. *PRX Quantum* **2022**, *3*, 010329. [CrossRef]
43. Mirrahimi, M.; Leghtas, Z.; Albert, V.V.; Touzard, S.; Schoelkopf, R.J.; Jiang, L.; Devoret, M.H. Dynamically protected cat-qubits: A new paradigm for universal quantum computation. *New J. Phys.* **2014**, *16*, 045014. [CrossRef]
44. Nigg, S.E. Deterministic Hadamard gate for microwave cat-state qubits in circuit QED. *Phys. Rev. A* **2014**, *89*, 022340. [CrossRef]
45. Yi, X.; Yang, Q.F.; Zhang, X.; Yang, K.Y.; Li, X.; Vahala, K. Single-mode dispersive waves and soliton microcomb dynamics. *Nat. Commun.* **2017**, *8*, 14869. [CrossRef]
46. Yang, C.P.; Su, Q.P.; Zheng, S.B.; Nori, F.; Han, S. Entangling two oscillators with arbitrary asymmetric initial states. *Phys. Rev. A* **2017**, *95*, 052341. [CrossRef]
47. Wang, Z.; Pechal, M.; Wollack, E.A.; Arrangoiz-Arriola, P.; Gao, M.; Lee, N.R.; Safavi-Naeini, A.H. Quantum Dynamics of a Few-Photon Parametric Oscillator. *Phys. Rev. X* **2019**, *9*, 021049. [CrossRef]
48. Puri, S.; Boutin, S.; Blais, A. Engineering the quantum states of light in a Kerr-nonlinear resonator by two-photon driving. *NPJ Quantum Inf.* **2017**, *3*, 18. [CrossRef]
49. Goto, H. Universal quantum computation with a nonlinear oscillator network. *Phys. Rev. A* **2016**, *93*, 50301. [CrossRef]
50. Grimm, A.; Frattini, N.E.; Puri, S.; Mundhada, S.O.; Touzard, S.; Mirrahimi, M.; Girvin, S.M.; Shankar, S.; Devoret, M.H. Stabilization and operation of a Kerr-cat qubit. *Nature* **2020**, *584*, 205–209. [CrossRef] [PubMed]
51. Yurke, B.; Stoler, D. The dynamic generation of Schrödinger cats and their detection. *Phys. B+C* **1988**, *151*, 298–301. [CrossRef]
52. Leghtas, Z.; Touzard, S.; Pop, I.M.; Kou, A.; Vlastakis, B.; Petrenko, A.; Sliwa, K.M.; Narla, A.; Shankar, S.; Hatridge, M.J.; et al. Confining the state of light to a quantum manifold by engineered two-photon loss. *Science* **2015**, *347*, 853–857. [CrossRef] [PubMed]
53. Sugawa, S.; Salces-Carcoba, F.; Perry, A.R.; Yue, Y.; Spielman, I.B. Second Chern number of a quantum-simulated non-Abelian Yang monopole. *Science* **2018**, *360*, 1429–1434. [CrossRef] [PubMed]
54. Weber, T.; Fobes, D.M.; Waizner, J.; Steffens, P.; Tucker, G.S.; Böhm, M.; Beddrich, L.; Franz, C.; Gabold, H.; Bewley, R.; et al. Topological magnon band structure of emergent Landau levels in a skyrmion lattice. *Science* **2022**, *375*, 1025–1030. [CrossRef] [PubMed]